CARBON 50 (2012) 1659–1666

Available at www.sciencedirect.com

SciVerse ScienceDirect

journal homepage: www.elsevier.com/locate/carbon

The effects of interlayer mismatch on electronic properties of bilayer armchair graphene nanoribbons

You Qian, Kai-Tak Lam, Chengkuo Lee, Gengchiau Liang *

Department of Electrical and Computer Engineering, National University of Singapore, 4 Engineering Drive 3, Singapore

ARTICLE INFO

Article history:
Received 9 June 2011
Accepted 4 December 2011
Available online 9 December 2011

ABSTRACT

We investigate the impact of interlayer mismatch on the electronic properties of bilayer graphene nanoribbons (BGNRs) with armchair-edges in terms of the total energy and electronic structures by first principle calculations. Simulation results show that in-plane misalignments require little energy and a large variation in the energy bandgap (E_G) can be observed. Based on the resulting atomic configurations due to the misalignments, the details of the observed relationship between bandgap and the lattice mismatch are investigated. It is observed that in general, misalignment in the transverse direction results in a decrease in the interaction between the two layers, giving rise to a larger E_G. On the other hand, misalignment in the longitudinal direction, i.e. along the edges, leads to an oscillation in E_G due to the periodic change of the GNR stacking order. A combination of these movements results in a complex variation of E_G, which introduces great uncertainty in electronic devices. However, such a phenomenon could also be used in various kinds of nanoelectromechanical systems as it provides a large change in electronic properties with a small movement.

1. Introduction

With unique properties such as high mobility and stable structure, two-dimensional graphene sheet has attracted a lot of attention in high performance electronic applications [1–9]. However, its zero bandgap (E_G) leads to a high OFF-state current in graphene transistors, making them not suitable for low-power digital circuits [10], and high performance FETs [11–17]. On the other hand, the electrons in the one-dimensional graphene nanoribbon (GNR) experience quantum confinement due to the presence of the edges, resulting in an usable E_G for digital device applications. Therefore, many experimental research efforts focus on fabricating GNRs, such as using photolithographic patterning and etching on a large graphene sheet [18,19] or chemical vapor deposition process [20,21].

However, these two approaches cannot make nano-width GNRs with smooth edges. As the width and edge roughness have a great effect on the electrical properties of GNRs [22,23], it is important to have precise control of these parameters. In this regard, a novel method was recently developed whereby single- or multi-wall carbon nanotubes (CNTs) are 'unzipped' by plasma etching [24] or chemical attack [25] to produce GNRs with relatively smooth edges. In particular, these approaches can possibly make bilayer GNRs (BGNRs) from double-wall CNTs as shown in Fig. 1. Apart from edge roughness and ribbon width, E_G of BGNRs is also highly sensitive to interlayer distance [26] and stacking position of the layers [27].

While the two layers of GNR should naturally be arranged in *AB-α* stacking (Bernal stacking) as shown in experimental studies [28], mismatch of these two layers may happen in the unzipping process and other high energy procedures, such as plasma or chemical etching used to obtain high quality BGNRs, and other forms of stacking, i.e. AA stacking, have

* *Corresponding author.*
E-mail address: elelg@nus.edu.sg (G. Liang).
0008-6223/$ - see front matter
doi:10.1016/j.carbon.2011.12.007

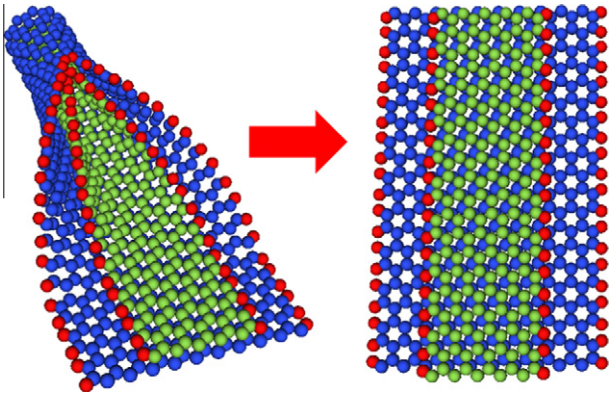

Fig. 1 – Unzip a double-walled carbon nanotube (DWCNT) to obtain a bilayer graphene nanoribbon (BGNR). The blue and green atoms represent the carbon atoms in CNT (10,0) and CNT (5,0), respectively, and the red atoms are hydrogen atoms. (For interpretation of the references to color in this figure legend, the reader is referred to the web version of this article).

been reported [29]. Furthermore, during device fabrication, the formation of contacts on BGNRs to connect with other components may exert an external force on the BGNRs, resulting in further mismatch of the two layers. As the electronic properties, in particular the E_G of BGNRs are highly sensitive to the stacking order, this lattice mismatch would greatly affect the conductance of the material and the performance of devices relying on bandgap modulations [30–32].

It is therefore important to look into how the external energy or force would affect the arrangement of BGNRs, as well as the impact of the layer mismatch on the electronic properties of BGNRs. This would give us a better understanding on the properties of BGNRs and, in extension, to multilayer GNRs with perfect structure impacted with external turbulent or excitation. Considering the stable honeycomb structure and strong C–C bond inside each layer, we focus on the change in the relative positions of the two GNR layers. In this paper, we examine the total energy of BGNRs by changing the arrangement of the top and bottom layer of BGNRs, which would help us to understand the influence of external energy. In addition, E_G at each of the corresponding mismatch point is obtained to investigate the misalignment effect on the electronic structure. We observed that the variation in total energy is below the level of thermal energy at room temperature, signifying that it is difficult to control the lattice alignment exactly, i.e. these layers could be easily moved by external force. Furthermore, the variation in E_G for different alignment is in the range of 0.7 eV for one of the cases, and we provide a hypothesis to explain this variation which can also be used to predict the E_G range of mismatched BGNRs with different widths.

2. Method

We investigate armchair-edge BGNRs with various interlayer lattice mismatch using *ab initio* calculations based on the density functional theory formulism as implemented in the software package ATOMISTIX TOOLKIT [33]. The Perdew–Zunger local density approximation (LDA) to the exchange correlation functional is used and the effect of the core electrons are described with the norm-conserving pseudo-potentials provided. We have assumed the material to be spin degenerate and the double-ζ basis set is used for the valence electrons. The k-point sampling is done via the Monkhorst–Pack method with 50 points in the *y*-direction (infinite) and 1 in the *x*- and *z*-directions. A padding of 10 Å is added in the superlattice in the *x*- and *z*-directions to emulate the one-dimensional system. The cut-off energy for carbon is set to 2 keV and we carried out atomic relaxation of monolayer GNR of 1.1 nm which results in a C–C bond length of 1.42 Å [34]. The main reason for choosing LDA over generalized gradient approximation (GGA) is attributed to the fact that GGA gives a weak bonding between graphene layers and results in a large value of interlayer distance. By contrast, LDA provides a good match with the results of graphite. Although LDA underestimates the bandgap, in this work, we focus on the variations in energy and the bandgap, and these changes with respect to the modifications in atomic structure are still indicative of the physics involved.

There are two conditions considered in this work: one with same ribbon width of 1.1 nm for top and bottom layers, and the other with different widths of 1.1 and 2.3 nm for the top and bottom layers, respectively. We examine firstly the same width case to understand the essential mechanism, before expending the investigation to a more realistic case where a double-wall CNT is made up of tubes with different diameters.

The width of an armchair-edge GNR is related to the number of carbon atoms (N) in the transverse direction. The 1.1 nm layer ($N = 10$) could be obtained from a perfectly unzipped CNT (5,0) in the longitudinal direction. Similarly, the 2.3 nm layer ($N = 20$) could be obtained from an unzipped CNT (10,0). In both situations, the GNRs are edge-passivated with hydrogen atoms, with initial C–C and C–H bond lengths of 1.42 and 1.09 Å, respectively. To perform the mismatch in different position, the bottom layer is anchored and the top layer is manually moved in various directions with respect to the bottom layer. The different layer arrangements are shown in Fig. 2(a)–(d) and the calculated energy difference and E_G at each mismatch locations are presented in Fig. 2(e) and (f), respectively. Before calculating the electronic structure, the optimal interlayer distance is determined by searching for the minimal total energy configuration as the interlayer distance varies. Lastly, the whole system would be relaxed until the force between each atom is less than 0.05 eV/Å and we note that this step would mainly relax the bonding length within each layer.

The start point of the structure for both cases [(0,0) in Fig. 2(e)] is *AA* stacking [Fig. 2(a)], with the two layers having the same coordinates in the longitudinal and transverse direction. The top layer would be moved across in the transverse direction (*x*-direction) until the two layers no longer overlapping each other. In the longitudinal direction (*y*-direction), as we have assumed that the layers are infinite in length, it is impossible to swap through all the possible positions. However, we only need to perform the calculation from 0 to 2.13 Å in the *y*-direction, which is one-and-a-half of the C–C bond length. From 2.13 to 4.26 Å, all the electronic properties is a mirror image of the previous region, with the mirror

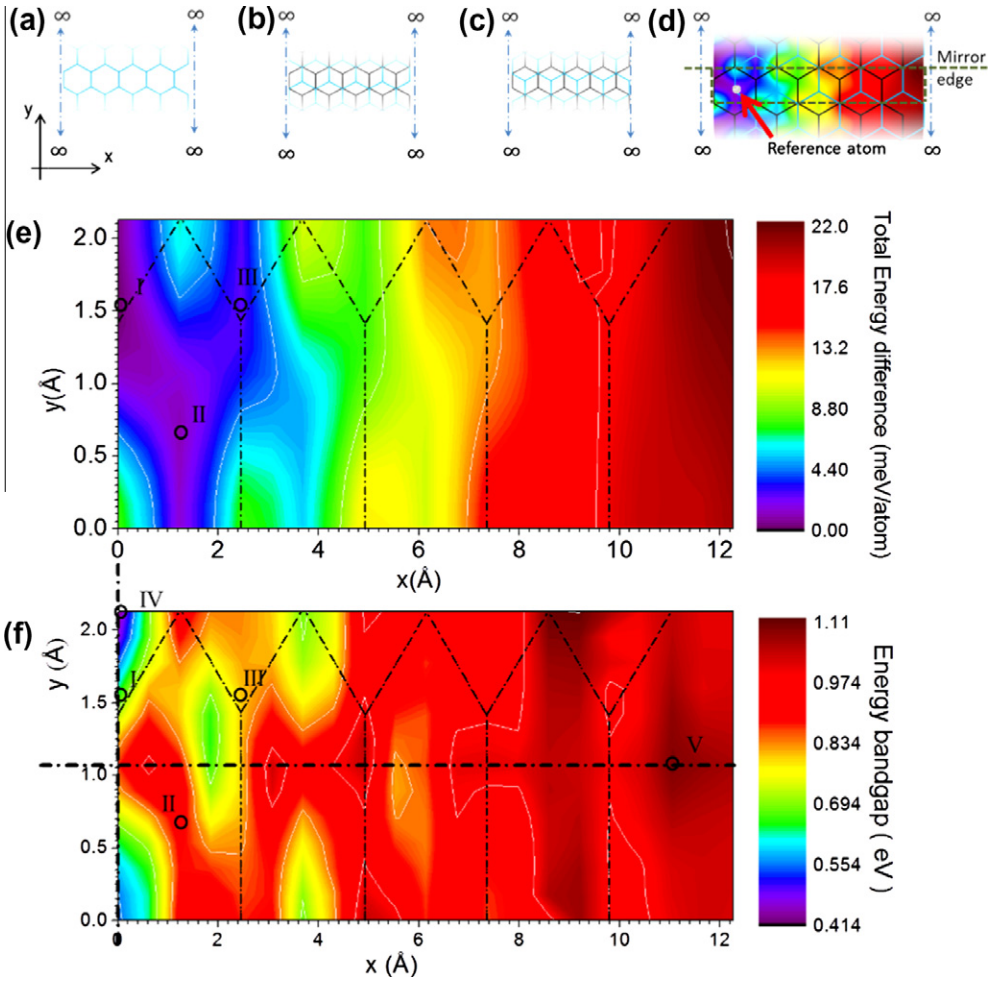

Fig. 2 – The wire-mesh representation of BGNR consisting of two 10-GNRs in (a) *AA* stacking, (b) *AB*-α stacking (Bernal stacking) and (c) *AB*-β stacking. In the longitudinal direction (*y*-direction), the BGNRs is infinite in length, and in the transverse direction (*x*-direction), the number of dimmer lines (*N*) is 10. The blue and black wire-meshes represent the top and bottom layers, respectively. (d) The change in total energy is represented in a contour plot with the coordinate in the plot representing the position of the reference atom, for example Point (0, 0) means the two layers are totally overlapped as in (a). A zoom-in of the unique region surrounded by the dash box is shown in (e). Point I (0, 1.59), Point II (1.23, 0.71) and Point III (2.46, 1.59) have the lower energy than the surrounding mismatch locations. The corresponding energy bandgap (E_G) of the unique region is shown in (f). (For interpretation of the references to colour in this figure legend, the reader is referred to the web version of this article).

edge at y = 2.13 Å [cf. Fig. 2(d)]. While the atomic structures of the two corresponding points in the mirror images does not looks similar in the top view, the bottom view of one point is same as the top view of the other, which is the reason for the mirror images observed. For areas farther away, i.e. $y > 4.26$ Å or $y < 0$ Å, the calculated properties are periodic with a unit length of 4.26 Å.

3. Results and discussion

3.1. *Same width case*

The top layer initial position is totally overlapped with the bottom layer as shown in Fig. 2(a), and the lattice mismatches in the *y*-direction are shown in Fig. 2(b) and (c), while the mismatch in *x*-direction is shown in Fig. 2(d). We only consider the top layer moving in two dimensions without any rotation. The axes in the contour plot on both Fig. 2(e) and (f) refer to the mismatch by using the reference atom indicated in Fig. 2(d).

3.1.1. *Variation in the total energy*

The total energy difference per atom, normalized to the lowest energy case, at different mismatch positions is shown in Fig. 2(d), with details corresponding to the region indicated by the dash line shown in Fig. 2(e). Three stable points are observed [I (0, 1.59), II (1.23, 0.71), III (2.46, 1.59)], where the total energies are lower than the surrounding mismatch locations. As opposed to the bilayer graphene, the lowest energy point I does not coincide with *AB* stacking. The small deviation from *AB* stacking is due to the influence of the hydrogen passivation at the edges, and the different observations from those

in bilayer graphene experiments could possibly occur. Furthermore, it is observed that the difference between the highest and the lowest energy point is 22 meV/atom, indicating a high probability for the GNR layers to shift in-plane with respect to each other under high-temperature annealing. As a result, without external interaction, it is difficult to determine the exact stacking and alignment of the BGNRs and a way to fix the two layers is required to obtain BGNRs with a particular alignment in experiment setups and device fabrications. On the other hand, the small total energy differences also suggest that movement between the two layers is easy to achieve and that the alignment of the BGNRs can be easily manipulate by inducing a small turbulence in the system.

3.1.2. *Variation in the energy bandgap*

Because of the small differences in total energy between the various alignments of the two layers, the electronic property in these situations is important as all of them are physically possible in room temperature. The E_G of the same width BGNR is calculated at the corresponding locations, shown in Fig. 2(f). For monolayer GNRs, the E_G is determined by N, where a smaller N usually gives a larger E_G due to stronger quantum confinement [34]. Monolayer GNRs also show three groups of E_G, with the $N = 3p + 2$ group having the smallest E_G, and the other two groups, 3p and 3p + 1, have relatively larger E_G. For BGNRs, the E_G is in general smaller than the monolayer GNR due to the weaker quantum confinement at the edges and the behavior of three groups is also shown in previous study [27]. In the current study, we concentrate on the impact of misalignment in the x- and y-direction on the E_G of the resulting system.

As shown in Fig. 2(f), the E_G varies as the relative positions of the GNR layers change. The E_G of the three picked points (I, II and III) are 0.624, 0.917, and 0.804 eV, respectively. The minimum E_G is obtained in the top-left corner [IV (0, 2.13)] at 0.414 eV, and the maximum E_G can be found in point V (11.07, 1.06) at 1.11 eV. The E_G variation is 0.696 eV for a small displacement, and especially near the left edge of the contour plot, the difference in E_G from point to point is quite remarkable. Furthermore, picking the largest (1.11 eV, point V) and smallest (0.414 eV, point IV) energy band gaps as example, the effective mass changes from 0.20 to 0.10 m_e, with m_e being the mass of electron. It implies that the carrier mobility would increase. Together with the smaller energy band gap, this results in a more conducting material.

We next investigate the E_G variation along $y = 1.07$ Å [c.f. Fig. 3(a)] where E_G shows large variations. It is found that although it has an oscillating pattern as x increases, the E_G approaches that of the monolayer GNRs ($E_G = 1.178$ eV) as x is large. This is because the interlayer interaction is smaller while the two layers have less overlap, and they behave more like two monolayer GNRs. To explain the anomaly at small x values (<7 Å), we focus on Point 1 in Fig. 3(a) ($x = 0.61$ Å). The atomic alignment at Point 1 is given in Fig. 3(b), where we consider the BGNR could be separated into three separate parts, two monolayer GNRs at the edges, which are emphasized with the red dashed rectangle, and a BGNR in the middle. The alignment at Point 1 shows two single layers in the edges corresponding to two $N = 1$ monolayer GNRs (1-GNRs), and an $N = 9$ BGNR (9-BGNR) in the middle. From previous classifications, the 1-GNR belongs to the family of 3p + 1 (although 1-GNRs is not physically feasible currently), and 9-BGNR belong to the family of 3p, both of which have a large E_G, which leads to an overall large E_G at Point 1. According to this, the whole structure could be considered as three separate parts, and by relating to the family each part belongs to, the E_G of the resulting structure can be estimated by the smallest E_G of the three parts. Similarly, Point 2 is corresponding to 2-GNRs at the edges, and 8-BGNR in middle [c.f. Fig. 3(c)]. Both of them belong to the 3p + 2 family, which has a smaller E_G, resulting in an overall small E_G material. Finally, at Point 3, there are two 3-GNRs (3p) at the edges and a 7-BGNR (3p + 1) in the middle, resulting in a large E_G similar to Point 1. The same behavior can be observed for other points such as Points 4, 5 and 6 as shown in Fig. 3(a). For even larger mismatch, as the decreasing interlayer interaction becomes a significant factor, i.e. the system resembles that of two separated monolayer GNRs, the trend is no longer periodic.

Next, we examine E_G variation along the line $x = 0$ [Fig. 4(a)], where the GNR layers are align in the transverse direction and only mismatches in the longitudinal direction are considered. At $y = 0$ [cf. Fig. 2(a)], representing *AA* stacking, E_G is small ($E_G = 0.544$ eV), and as y increases up to 1.07 Å [cf. Fig. 4(d)], E_G increases to a maximum of 0.871 eV. Further increase in y results in a decrease in E_G to a minimum of 0.414 eV at $y = 2.13$ Å, where a mirror image is observed afterward. The mismatches in the longitudinal direction is different from the previous case in that the two GNR layers are always overlapped, and hence there are less changes in the interlayer edge interaction. To isolate the effect of the change in lattice alignment from the effect of the change in interlayer edge interaction, we perform a similar calculation on bilayer graphene (BLG) where the edge effect is eliminated in the two-dimensional structure. The change in E_G of the BLG is shown in Fig. 4(b). It is observed that at Point 1, the *AA* stacking results in zero-E_G, and as the top layer moves in the y-direction, the interlayer interaction changes due to the change in the distances between the atoms in the top and bottom layers [30] and this opens a small bandgap ($E_G = 0.17$ eV at $y = 0.71$ Å, cf. Point 2) in BLG. Further increase in y results in a drop in the E_G back to 0 (cf. Point 3) which represent the *AB* stacking [Fig. 4(e)], and it stays at 0 due to the symmetry of the lattice where the distances between the carbon atoms in the top and bottom layers do not vary significantly [cf. Fig. 4(f) and Point 4]. While similar trends are observed in BGNR [cf. Fig. 4(a) and (b)], E_G in BGNR is much higher and it never drops to 0. This is mainly due to the quantum confinement at the edges. Furthermore, the peak point in BGNR is shifted to $y = 1.07$ Å and the up-slope and down-slope are less symmetrical as compared to those in BLG. This could be attributed to the presence of the hydrogen atoms at the edges which change the C–C bond lengths at the edges and break the lattice symmetry.

3.2. *Different width case*

Lastly, we investigate the case where the two GNR layers have different widths. Considering a perfectly unzipped double-walled CNT (DWCNT), it is natural to have two nanotubes with different diameters and hence BGNRs with different widths.

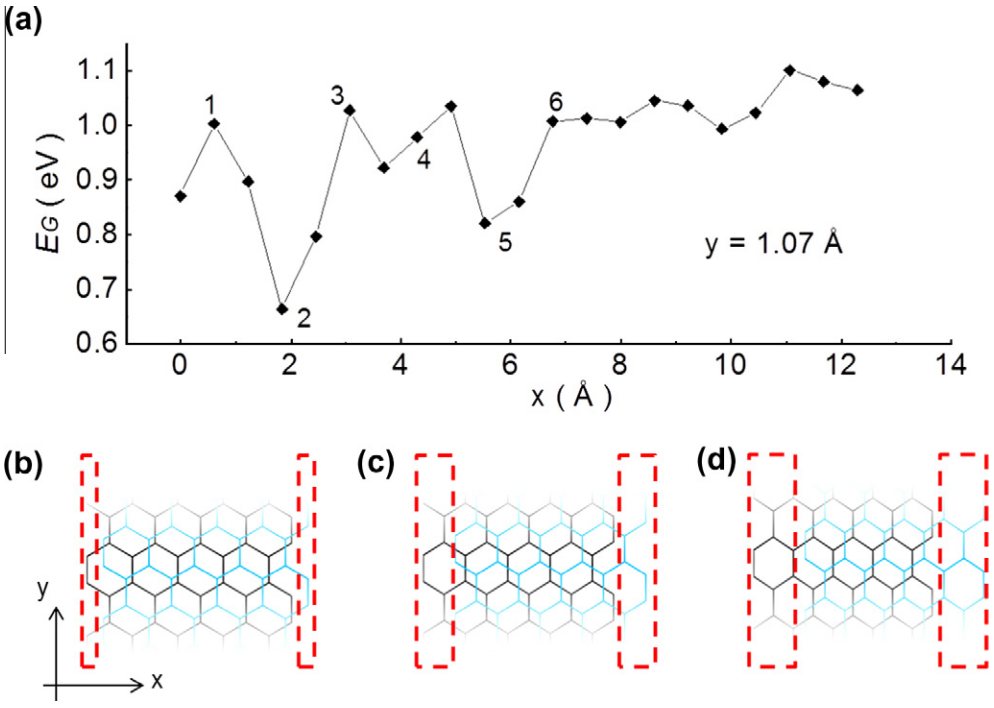

Fig. 3 – (a) The variation in E_G extracted along the line y = 1.07 Å for the same width BGNR case. The atomic configurations of Points 1–3 are shown in (b–d), respectively. The regions inside the red dash rectangles are the single layer GNR at the edges which, together with the BGNR in the middle, control the E_G of the lattice mismatched BGNR. (For interpretation of the references to colour in this figure legend, the reader is referred to the web version of this article).

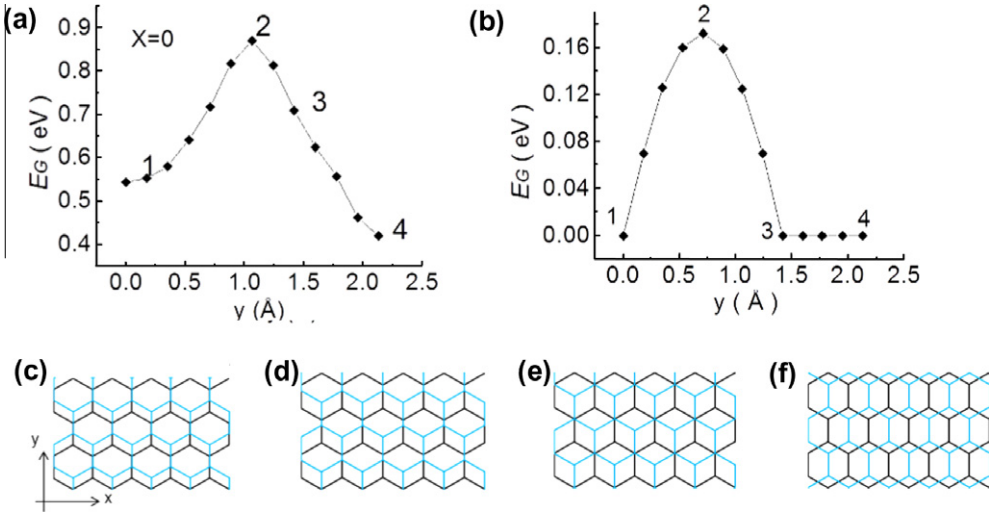

Fig. 4 – (a) The variation in E_G extracted along the line x = 0 Å for the same width BGNR case. (b) The variation in E_G of bilayer graphene. The atomic configurations at Points 1–4 are shown in (c–f), respectively.

We consider a DWCNT with CNT (5,0) and CNT (10,0), corresponding to 10-GNR and 20-GNR, respectively. In this case, we only let the $N = 10$ layer moves within the $N = 20$ bottom layer [cf. Fig. 5(a)] as we have already learnt from the previous section that moving the top layer out will obtain separated single layers behavior. A stronger periodic behavior is observed in both total energy and E_G, shown in Fig. 5(b) and (c), respectively. For the total energy plot, multiple stable (minimal energy) points could be observed which all represents *AB* stacking. However, as the maximum change in total energy is very small at 6.2 meV/atom, the top layer can be in any position and hence, similar to the same width case, external means are required to fix the relative position of the two layers. The variation in total energy is a mirror image along the mid-line, with a little difference at the two edges, which might be due to the hydrogen passivation at the edges of the top and bottom layers.

Similarly, the variation in E_G is also more periodic than that of the same width case, and the changes can be explained by the same reasons in the previous section. In the

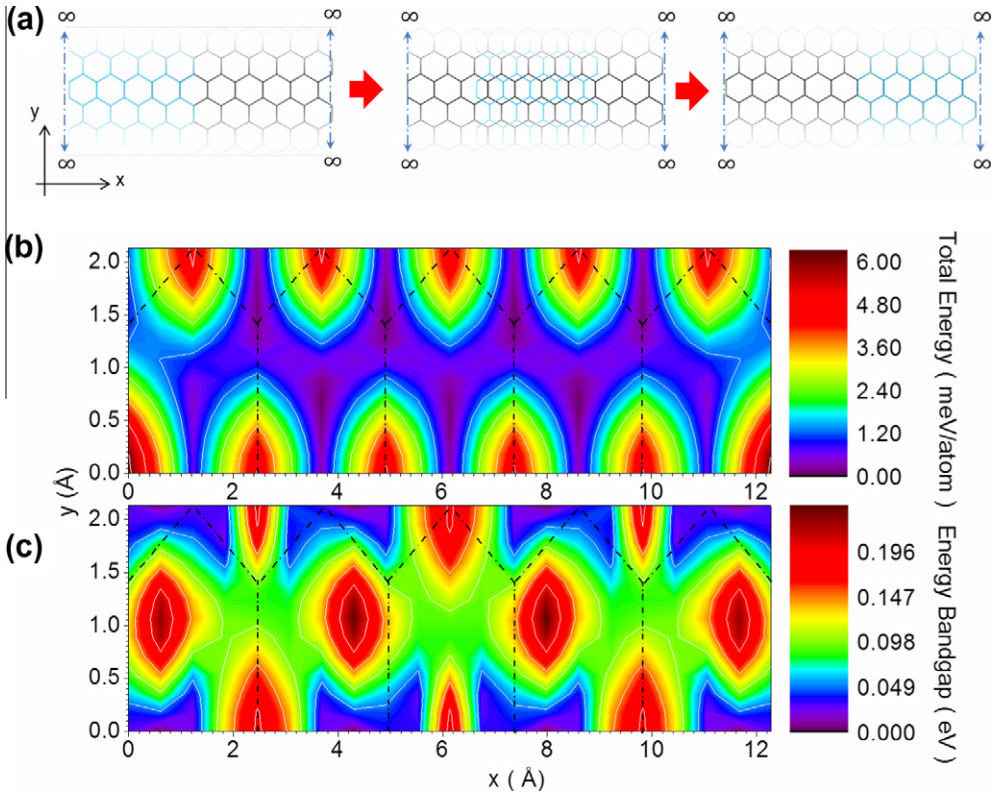

Fig. 5 – (a) The atomic configuration of BGNR consist a 10-GNR top layer and a 20-GNR bottom layer, with the top (blue) layers moving from the left to the right edges. Unlike the previous same width case, the top layer is always overlapped with the bottom layer. The contour plots of the change in total energy and the different E_G are shown in (b) and (c), respectively. (For interpretation of the references to color in this figure legend, the reader is referred to the web version of this article).

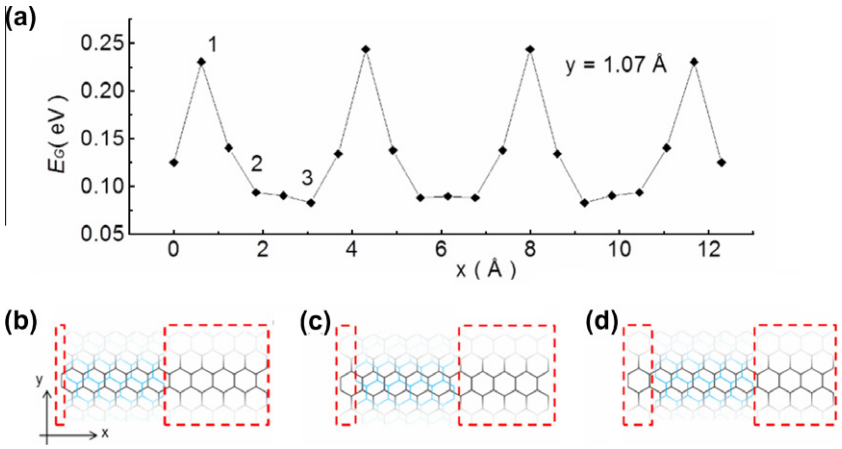

Fig. 6 – (a) The variation in E_G extracted along the line y = 1.07 Å for the different width BGNR case. The atomic configurations of Points 1–3 are shown in (b–d), respectively, with the red dash rectangles highlighting the single layer GNRs at the edges. (For interpretation of the references to colour in this figure legend, the reader is referred to the web version of this article).

same width case, the E_G varies from 0.4 to 1.05 eV while in the current case, it changes from almost 0 to 0.241 eV, as shown in Fig. 5(c). The general decrease in E_G is due to the $N = 20$ layer (3p + 2) having a much smaller E_G than the $N = 10$ layer. Although the monolayer 10-GNR has a large E_G of 1.21 eV and the monolayer 20-GNR has a small E_G of 0.1 eV, the maximum E_G of the bilayer system (0.24 eV) is an intermediate of these components. In the transverse direction, the E_G variation along y = 1.07 Å is plotted in Fig. 6(a). The overlap region involves a 10-GNR (3p + 1) at the top layer covering a 9-GNR (3p) at the bottom, shown in Fig. 6(b)–(d). Therefore, BGNR in the middle part could be considered as large bandgap material. For Point 1 in Fig. 6(a) [lattice arrangement shown in Fig. 6(b)], there are 1-GNR (3p + 1) and 10-GNR (3p + 1) at

the two edges, resulting in a large bandgap. Similarly for Point 2 [cf. Fig. 6(c)], there are 2-GNR (3p + 2) and 9-GNR (3p) at the edges. Since the 2-GNR belongs to the small E_G family, the resulting E_G is small. It also can be found that the same case happens for Point 3 [cf. Fig. 6(d)], where the 3-GNR (3p) and 8-GNR (3p + 2) at the edges give a small E_G.

4. Conclusions

We have explored the fundamental effects of lattice mismatch in BGNR in terms of total energy and energy bandgap. The energy difference between various mismatches is comparable to the thermal energy in room temperature, indicating that the relative position of the two layers is not stable if they are not anchored by external means. The E_G of BGNRs is largely influenced by the property of the constituent monolayer GNRs and their interactions, especially the one with smaller E_G. Furthermore, at small mismatch in the transverse direction where there are large overlap of the two layers, the E_G can be roughly predicted by dividing the BGNR into three parts, and then considering the family each part belongs to.

This comprehensive study on the change in E_G with respect to physical alignment provides an excellent opportunity in device designs. We observed that a shift of less than 0.1 nm between the layers triggers a change in E_G of about 0.5 eV which would lead to a change in the conductance of the material. This indicates the potential application in nanoelectromechanical (NEM) switches, where the ON- and OFF-state of the NEM switch could be obtained by creating the lattice mismatch. Considering the small change in total energy, a low power consumption NEM switch can be realized. Furthermore, the size of the devices could be as small as tenths of nanometers, which, coupled with the ultra-high sensitivity, would make BGNRs a suitable material in various types of sensor applications.

Acknowledgments

This work was supported by the Science and Engineering Research Council, Agency for Science, Technology and Research, Singapore, under Grant Nos. 102-101-0022 and 082-101-0023, and the Singapore National Research Foundation Competitive Research Program Fund. Computational resources are provided by the Computational Nanoelectronics and Nano-device Lab, Department of Electrical and Computer Engineering, National University of Singapore.

REFERENCES

[1] Wu Y, Lin YM, Bol AA, Jenkins KA, Xia F, Farmer DB, et al. High-frequency, scaled graphene transistors on diamond-like carbon. Nature 2011;472(7341):74–8.
[2] Liang GC, Neophytou N, Nikonov DE, Lundstrom MS. Performance projections for ballistic graphene nanoribbon field-effect transistors. IEEE Trans Electron Dev 2007;54(4):677–82.
[3] Lam KT, Seah D, Chin SK, Kumar SB, Samudra G, Yeo YC, et al. A simulation study of graphene-nanoribbon tunneling FET with heterojunction channel. IEEE Electron Dev Lett 2010;31(6):555–7.
[4] Kai-Tak L, Yue Y, Samudra GS, Yee-Chia Y, Gengchiau L. Electrostatics of ultimately thin-body tunneling FET using graphene nanoribbon. IEEE Electron Dev Lett 2011;32(4):431–3.
[5] Chin SK, Seah D, Lam KT, Samudra GS, Liang G. Device physics and characteristics of graphene nanoribbon tunneling FETs. IEEE Trans Electron Dev 2010;57(11):3144–52.
[6] Li X, Zhu Y, Cai W, Borysiak M, Han B, Chen D, et al. Transfer of large-area graphene films for high-performance transparent conductive electrodes. Nano Lett 2009;9(12):4359–63.
[7] Tung VC, Chen LM, Allen MJ, Wassei JK, Nelson K, Kaner RB, et al. Low-temperature solution processing of graphene-carbon nanotube hybrid materials for high-performance transparent conductors. Nano Lett 2009;9(5):1949–55.
[8] Wang DW, Li F, Zhao J, Ren W, Chen ZG, Tan J, et al. Fabrication of graphene/polyaniline composite paper via in situ anodic electropolymerization for high-performance flexible electrode. Acs Nano 2009;3(7):1745–52.
[9] Stoller MD, Park S, Zhu Y, An J, Ruoff RS. Graphene-based ultracapacitors. Nano Lett 2008;8(10):3498–502.
[10] Das A, Pisana S, Chakraborty B, Piscanec S, Saha SK, Waghmare UV, et al. Monitoring dopants by Raman scattering in an electrochemically top-gated graphene transistor. Nat Nanotechnol 2008;3(4):210–5.
[11] Ouyang YJ, Campbell P, Guo J. Analysis of ballistic monolayer and bilayer graphene field-effect transistors. Appl Phys Lett 2008;92(6):063120.
[12] Xia FN, Farmer DB, Lin YM, Avouris P. Graphene field-effect transistors with high on/off current ratio and large transport band gap at room temperature. Nano Lett 2010;10(2):715–8.
[13] Lin YM, Dimitrakopoulos C, Jenkins KA, Farmer DB, Chiu HY, Grill A, et al. 100-GHz transistors from wafer-scale epitaxial graphene. Science 2010;327(5966):662.
[14] Wu Y, Ye P, Capano MA, Xuan Y, Sui Y, Qi M, et al. Top-gated graphene field-effect-transistors formed by decomposition of SiC. Appl Phys Lett 2008;92:092102.
[15] Fiori G, Iannaccone G. On the possibility of tunable-gap bilayer graphene FET. IEEE Electron Dev Lett 2009;30(3):261–4.
[16] Lemme M, Echtermeyer T, Baus M, Szafranek B, Bolten J, Schmidt M, et al. Mobility in graphene double gate field effect transistors. Solid State Electron 2008;52(4):514–8.
[17] Meric I, Han MY, Young AF, Ozyilmaz B, Kim P, Shepard KL. Current saturation in zero-bandgap, top-gated graphene field-effect transistors. Nat Nanotechnol 2008;3(11):654–9.
[18] Han MY, Ozyilmaz B, Zhang YB, Kim P. Energy band-gap engineering of graphene nanoribbons. Phys Rev Lett 2007;98(20):206805.
[19] Liu L, Zhang YL, Wang WL, Gu CZ, Bai XD, Wang EG. Nanosphere lithography for the fabrication of ultranarrow graphene nanoribbons and on-chip bandgap tuning of graphene. Adv Mater 2011;23(10):1246–51.
[20] Campos-Delgado J, Romo-Herrera JM, Jia XT, Cullen DA, Muramatsu H, Kim YA, et al. Bulk production of a new form of sp(2) carbon: Crystalline graphene nanoribbons. Nano Lett 2008;8(9):2773–8.
[21] Li XL, Wang XR, Zhang L, Lee SW, Dai HJ. Chemically derived, ultrasmooth graphene nanoribbon semiconductors. Science 2008;319(5867):1229–32.
[22] Yoon Y, Guo J. Effect of edge roughness in graphene nanoribbon transistors. Appl Phys Lett 2007;91(7):073103.
[23] Basu D, Gilbert MJ, Register LF, Banerjee SK, MacDonald AH. Effect of edge roughness on electronic transport in graphene nanoribbon channel metal-oxide-semiconductor field-effect transistors. Appl Phys Lett 2008;92(4):042114.
[24] Jiao LY, Zhang L, Wang XR, Diankov G, Dai HJ. Narrow graphene nanoribbons from carbon nanotubes. Nature 2009;458(7240):877–80.

[25] Kosynkin DV, Higginbotham AL, Sinitskii A, Lomeda JR, Dimiev A, Price BK, et al. Longitudinal unzipping of carbon nanotubes to form graphene nanoribbons. Nature 2009;458(7240):872–6.
[26] Lam KT, Liang GC. An *ab initio* study on energy gap of bilayer graphene nanoribbons with armchair-edges. Appl Phys Lett 2008;92(22):223106.
[27] Sahu B, Min H, MacDonald AH, Banerjee SK. Energy gaps, magnetism, and electric-field effects in bilayer graphene nanoribbons. Phys Rev B 2008;78(4):045404.
[28] Castro EV, Novoselov KS, Morozov SV, Peres NMR, Dos Santos JMBL, Nilsson J, et al. Biased bilayer graphene: semiconductor with a gap tunable by the electric field effect. Phys Rev Lett 2007;99(21): 216802.
[29] Liu Z, Suenaga K, Harris PJF, Iijima S. Open and closed edges of graphene layers. Phys Rev Lett 2009;102(1):015501.
[30] Lam KT, Lee C, Liang G. Bilayer graphene nanoribbon nanoelectromechanical system device. A computational study. Appl Phys Lett 2009;95(14):143107.
[31] Lam KT, Liang GC. A computational evaluation of the designs of a novel nanoelectromechanical switch based on bilayer graphene nanoribbon. In: 2009 IEEE international electron devices meeting, Washington, DC, USA. IEEE, 2009; 841–4.
[32] Gonzalez JW, Santos H, Pacheco M, Chico L, Brey L. Electronic transport through bilayer graphene flakes. Phys Rev B 2010;81(19):195406.
[33] QAS. Atomistix ToolKit Manual "ATK version 2008.10".
[34] Son YW, Cohen ML, Louie SG. Energy gaps in graphene nanoribbons. Phys Rev Lett 2006;97(21):216803.